Investigation of Bubble Plume Oscillations by Euler-Euler Simulation

Fleck, S.; Rzehak, R.;

Originally published:

July 2019

Chemical Engineering Science 207(2019), 853-861

DOI: https://doi.org/10.1016/j.ces.2019.07.011

Investigation of Bubble Plume Oscillations by Euler-Euler Simulation

Sebastian Fleck[1,2], Roland Rzehak[1*]

[1] Helmholtz-Zentrum Dresden – Rossendorf, Institute of Fluid Dynamics, Bautzner Landstrasse 400, D-01328 Dresden, Germany
[2] Technische Universität Dresden, Chair of Chemical Reaction Engineering and Process Plant, Münchnerplatz 3, D-01062 Dresden, Germany

Abstract

For practical applications the Euler-Euler two-fluid model relies on suitable closure relations describing interfacial exchange processes. An ongoing effort at HZDR has led to a validated set of closures for adiabatic bubbly flows that is applicable under a rather broad range of conditions including flows in pipes and bubble columns. Up to now, however, only flows with stationary mean values have been considered. The present contribution extends the model validation to dynamic flow phenomena by considering a periodically oscillating bubble plume. Consequently, the turbulence model then runs in URANS mode. Literature data for a partially aerated flat rectangular bubble column are used for comparison. In particular, results for the plume oscillation period show good agreement between simulation and experiment.

Keywords: bubble columns, dispersed gas liquid multiphase flow, Euler-Euler two fluid model, closure relations, CFD simulation, model validation

* Corresponding author. E-mail: r.rzehak@hzdr.de

TABLE OF CONTENTS

1 INTRODUCTION

Bubbly flows are common in many engineering disciplines comprising chemical engineering, mineral processing, and biotechnology. The fluid dynamics of such systems displays complex behavior for which to date only partial understanding is available. Consequently, design and optimization of technical equipment involving bubbly flow present a great challenge. In this situation, CFD simulations bear the potential of identifying energy- and resource- efficient solutions which are prohibitively expensive and time-consuming to uncover by conventional semi-empirical methods.

CFD simulations of dispersed bubbly flow on the scale of technical equipment are feasible within the Eulerian two-fluid framework of interpenetrating continua. Since phenomena occurring on the scale of individual bubbles or groups thereof are not resolved in this approach, accurate numerical predictions rely on suitable closure relations describing the physics of these small- scale phenomena. As a first step towards a predictive model, a set of baseline closures applicable to adiabatic bubbly flows has been proposed in Rzehak and Krepper (2013) comprising the exchange of momentum between gas and liquid phases and the effects of the dispersed bubbles on the turbulence of the liquid carrier phase. Comparisons between different model alternatives were made to select the most promising candidate for less deeply investigated submodels (Rzehak et al. 2012, Rzehak and Krepper 2013a). Subsequently this baseline model has been applied to a number of diverse test cases to assure its validity for a broad range of conditions (Rzehak et al. 2017, Shi and Rzehak 2018 and references therein). This is a prerequisite to facilitate reliable predictions in situations where no data exist against which the model results could be compared, such that it is not possible to make adjustments and the model has to be used in exactly the way it was proposed. This venture is continued in the present work.

For the purpose of model validation it is vital that in addition to local values of the phase fraction and velocity fields, information on the bubble size is available as well, since virtually all of the closure models used in Euler-Euler simulations depend on this variable. Moreover, some parametric variation of its value would be desirable in order to make a meaningful comparison between different models. Data selected according to these criteria have been used in the validation studies mentioned above. However, only flows with stationary mean values were considered so far. The purpose of the present work is to extend the validation of the baseline model to a dynamic flow situation, namely a periodically oscillating bubble plume. This is a flow pattern that develops in bubble columns with localized gas injection as sketched in Figure 1 below. In these devices the average motion of the gas stream emanating from the sparger is not in a straight vertical path, but instead it is deflected sidewards. If the depth of the column is rather thin and the fill height exceeds a certain level, a periodic oscillation occurs between deflection to either side along the column width. This presents a time-dependent flow in which the period of the plume oscillations provides a measure to validate the dynamic predictions of the baseline model.

Early observations of the basic phenomena were made by Lin et al. (1996), Delnoij et al. (1997), Becker et al. (1999), and Pfleger et al. (1999). Mainly the dependence of the period of the bubble plume oscillations on the gas volume flux was studied. Rensen and Roig (2001) cast their own and previous experimental data for the dependency of the plume oscillation period on various system parameters in dimensionless form. Buwa and Ranade (2002, 2004, 2005) conducted a rather comprehensive study which included spargers producing bubbles

of different size in addition to varying aspect ratio (i.e. fill height over column width) and gas flow rate. Based on their own and previous data they also proposed a correlation for the plume oscillation period in dimensionless form. Diaz et al. (2006, 2008) focused on characterizing the regimes of oscillating as opposed to stationary plumes in terms of aspect ratio and gas flow rate. An oscillating plume was found if the aspect ratio exceeded a certain value around 2 while under this condition the oscillation period did not depend appreciably on the aspect ratio. A more recent investigation in this line was made by Upadhyay et al. (2013) based on the newly available technique of Computer Aided Radioactive Particle Tracking (CARPT). The experiments of Julia et al. (2007) considered variation of the size of the sparged region and the crossover between partially and fully aerated columns. Cachaza et al. (2011) and Laupsien et al. (2017) performed experiments to investigate effects of material properties, namely surface tension and viscosity, respectively. With the exception of surface tension, all parameters were included in the experiments of Liu et al. (2019). A correlation for the plume oscillation frequency was given in that work as well.

Some of the previous studies also contained results from simulations of the respective setup. Delnoij et al. (1997) applied the Euler-Lagrange framework accounting for drag, lift, and virtual mass forces acting on the bubbles. No turbulence was considered in either phase. Pfleger et al. (1999) employed the Euler-Euler framework with a single phase k-ε turbulence model for the liquid and turbulent dispersion was included by a diffusive term in the continuity equation. Only the drag force was taken into account. The work of Buwa and Ranade (2002) was again based on the Euler-Euler framework, for some of the calculations coupled with a population-balance equation. Again a single phase k- ε turbulence model was used for the liquid and turbulent dispersion was included by a diffusive term in the continuity equation. Forces acting on the bubbles, however, comprised in addition to drag also lift and virtual mass forces. A few further works devoted entirely to simulations have appeared as well. Buwa et al. (2006) showed Euler-Lagrange simulations of their experiments with similar modeling of bubble forces as liquid phase turbulence as in their earlier Euler-Euler simulations. Turbulent dispersion was modeled by a discrete random walk model. Gupta and Roy (2013) investigated the setup of Upadhyay et al. (2013) by a coupled Euler-Euler population-balance framework. Drag, lift, and virtual mass force were considered and a RNG k- ε turbulence model was applied to the gas-liquid mixture.

As may be seen, the previous simulations have used rather different overall approaches and different submodels for specific effects. This makes it difficult to select an appropriate model for future applications, in particular where true predictions are sought (i.e. no data are available). Therefore it is advantageous to apply the baseline model introduced at the outset, and this is the objective of the present work. From the available experimental data, the study of Buwa and Ranade (2002, 2004, 2005) comes closest to the criteria defined above, and hence this is chosen as the core of the comparison. Supplementary data for very similar configurations are taken from Pfleger et al. (1999) and Diaz et al. (2006) as well as Darmana et al. (2007), a study that focused more on mass transfer and chemical reaction, but also has data on the plume oscillations. A description of these experiments is given in section 2. The applied baseline model is summarized in section 3 with references to more detailed presentations that have been given previously. The simulation results are then presented in section 4 and compared to the measurements. The comparison with the data from Darmana et al. (2007) is taken from an earlier simulation study using the same model as the present one (Krauß and Rzehak 2018). Conclusions are offered in section 5.

2 SUMMARY OF EXPERIMENTAL DATA

In a series of works Buwa and Ranade (2002, 2004, 2005) investigated flows in a thin rectangular bubble column with localized gas injection in the center of the bottom plate as sketched in Figure 1. In all cases the aspect ratio of the column (i.e. the ratio of fill height to width, H/D) was larger than 2, such that an oscillating bubble plume develops (e.g. Diaz et al. 2006). The main parameters that were varied in the experiments are gas flow rate and aspect ratio. The former assumed values between J_G= 0.14 and 0.73 cm/s. For the latter, a lower value was H/D = 2.25 and a higher value was in the range H/D = 4.5 … 5.5. In addition, two different types of spargers were used, where one consisted of a perforated plate with 8 individual holes, the other one was a sintered disc. The main difference between the two sparger types was that they produced bubbles of different size. Details of the arrangement did not show appreciable effects. Air was used for the gas and tap water for the liquid. Temperature and pressure are not specified explicitly but presumably were at ambient values.

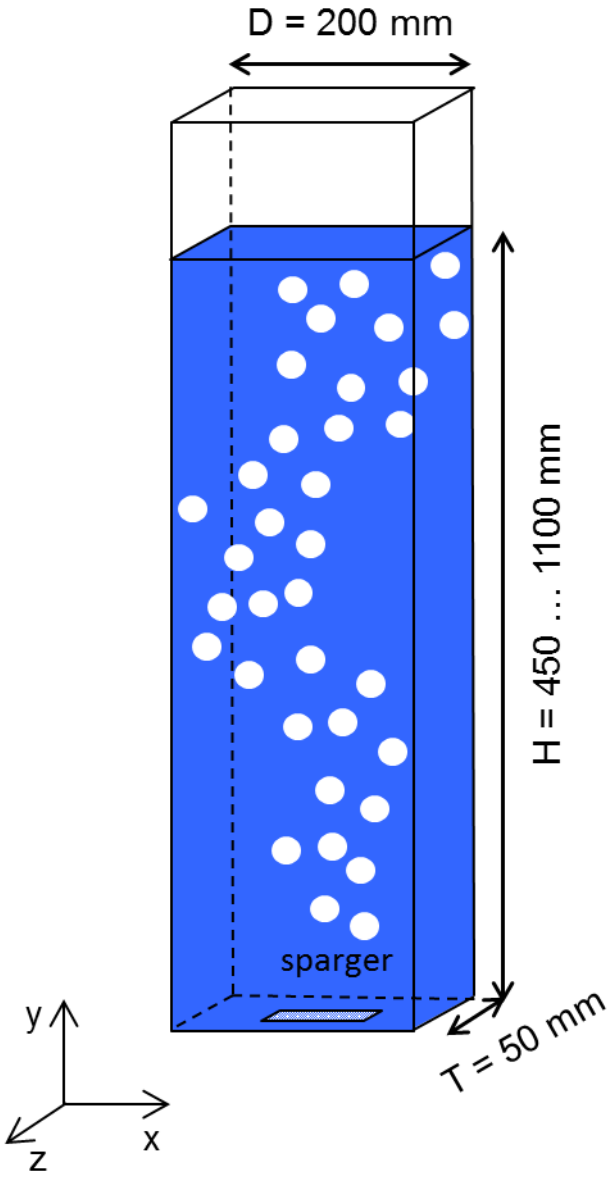

Figure 1: Sketch of the bubble column geometry.

The plume oscillation frequency was found by applying a Fourier transform to a time series of fluctuating wall pressure in Buwa and Ranade (2002) and of fluctuating gas fraction in Buwa and Ranade (2004). Bubble sizes were determined in Buwa and Ranade (2002) using high speed digital photography. Measurements of gas fraction were taken along lateral profiles in the mid-plane of the channel at various axial locations above the inlet in Buwa and Ranade (2002, 2005) by a conductivity probe.

Additional data on oscillating bubble plumes are available from several other sources. Profiles of the mean liquid velocity were obtained in Pfleger et al. (1999) by means of LDA for a setup matching the one of Buwa and Ranade (2002, 2004, 2005) with the perforated plate sparger. Data on the total gas fraction are given in Diaz et al. (2006) for a column which measures only 40 mm in depth, but otherwise has the same geometry as Buwa and Ranade (2002, 2004, 2005) and Pfleger et al. (1999). Finally, mean gas velocity profile and plume oscillation frequency were reported by Darmana et al. (2007) for N2 bubbles in aqueous NaOH solution in a bubble column with an aspect ratio of 5, a depth of 30 mm, and a sparger consisting of 21 needles. The gas volume flux was 0.7 cm/s and the bubble size 5.5 mm in these experiments. The slight variations in the experimental conditions of Diaz et al. (2006) and Darmana et al. (2007) appear to have at most a minor impact on the large scale features of the flow under investigation here.

3 MODEL DESCRIPTION AND NUMERICAL SETUP

The physical models used for the simulations are exactly the same as used in a number of previous studies. Since extensive descriptions have been presented repeatedly, only a rather concise summary is given here for the sake of completeness together with references to the original works. Material properties, geometry, and boundary conditions suitable for the present application are specified in detail.

The conservation equations for two-phase flow are summarized as follows (e.g. Drew and Passman 1998, Yeoh and Tu 2010, Ishii and Hibiki 2011).

The phasic continuity equations read

$$\frac{\partial}{\partial t}(\alpha_G \rho_G) + \nabla \cdot (\alpha_G \rho_G \boldsymbol{u}_G) = 0 \tag{1}$$

$$\frac{\partial}{\partial t}(\alpha_L \rho_L) + \nabla \cdot (\alpha_L \rho_L \boldsymbol{u}_L) = 0 \,, \tag{2}$$

while the phasic momentum equations are

$$\frac{\partial}{\partial t}(\alpha_G \rho_G \boldsymbol{u}_G) + \nabla \cdot (\alpha_G \rho_G \boldsymbol{u}_G \otimes \boldsymbol{u}_G) = -\alpha_G \nabla p_G + \nabla \cdot (\alpha_G \mathbf{T}_G) + \alpha_G \rho_G \boldsymbol{g} + \boldsymbol{F}_G^{inter} \tag{3}$$

$$\frac{\partial}{\partial t}(\alpha_L \rho_L \boldsymbol{u}_L) + \nabla \cdot (\alpha_L \rho_L \boldsymbol{u}_L \otimes \boldsymbol{u}_L) = -\alpha_L \nabla p_L + \nabla \cdot (\alpha_L \mathbf{T}_L) + \alpha_L \rho_L \boldsymbol{g} + \boldsymbol{F}_L^{inter} \,. \tag{4}$$

The terms $\boldsymbol{F}^{inter}$ in Eqs. (3) and (4) account for the momentum transfer between the phases. Due to momentum conservation the relation $\boldsymbol{F}_G^{inter} = -\boldsymbol{F}_L^{inter}$ holds. According to the baseline model applied herein, the interphase force comprises of a number of contributions summarized in Table 1 together with the closure correlation used for each. Further details and validation studies can be found e.g. in Ziegenhein et al. (2013), Rzehak et al. (2015), Liao et al. 2016, Rzehak and Krepper (2015), or Rzehak et al. (2017a).

Table 1: Summary of bubble force correlations.

force	reference
drag	Ishii and Zuber (1979), single bubbles
shear lift	Tomiyama et al. (2002)
wall lift	Hosokawa et al. (2002)
turbulent dispersion	Burns et al. (2004)
virtual mass	constant coefficient C_{VM} = ½

The stress tensor

$$\mathbf{T} = \left(\mu + \mu^{turb}\right)(\nabla \boldsymbol{u} + (\nabla \boldsymbol{u})^T) \tag{5}$$

comprises both viscous and turbulent contributions. For the liquid phase, the turbulent dynamic viscosity μ_L^{turb} is calculated from a k-ω SST model with additional source terms accounting for the bubble- induced turbulence. Due to the low density and small spatial scales of the bubbles, turbulence may be neglected for the gas phase by setting $\mu_G^{turb} = 0$.

Further details on the turbulence modeling are given e.g. in Rzehak and Krepper (2013a), Rzehak and Kriebitzsch (2015), Ziegenhein et al. (2017) or Parekh and Rzehak (2018).

To obtain a complete system of equations additional relations are needed. Assuming each phase to be incompressible, these are an expression for the overall conservation of volume, $\alpha_G + \alpha_L = 1$, and the assumption of pressure equilibrium, $p_G = p_L = p$.

The material properties used correspond to air bubbles in water at atmospheric pressure and 25°C temperature and are summarized in Table 2.

Table 2: Summary of material properties.

ρ_L	997	kg / m³
μ_L	8.899e-4	kg / (m s)
ρ_G	1,185	kg / m³
μ_G	1.831e-5	kg / (m s)
σ	0.072	N / m

The simulations are performed using the commercial software ANSYS CFX 17.2. The full volume of the column up to the ungassed fill height is considered as the computational domain. A degassing boundary condition is applied at the top of the domain. The sparger is modeled as a region of 24 x 12 mm size in the center of the bottom of the domain on which an inlet boundary condition is prescribed. The area of this region corresponds to the area occupied by the sparger in the experiment, while details of the arrangement of the holes are neglected. The gas flux through this area is set to the desired value for the case under consideration. On the rest of the bottom as well as on the side walls of the domain, a no-slip condition is used for the liquid phase and a free-slip condition for the gas phase, assuming that direct contacts between the bubbles and the walls are negligible. To avoid the need to resolve the viscous sub-layer, a single phase turbulent wall function assuming a smooth wall is applied which consists of a blend between inertial and viscous sub-layers (referred to as “automatic wall-function treatment” in the ANSYS-CFX user guide). Simulations are run in a time-dependent mode corresponding to an URANS treatment of turbulence (Ziegenhein et al. 2017). As a consequence, time-averaging is applied to all quantities. A grid spacing of ~3 mm in all space directions was determined as suitable in a grid independence study. In Figure 2 and Figure 3 results for a finer grid with ~2 mm grid spacing are shown for comparison. Deviations between results for the vertical component of liquid velocity and gas fraction on both grids are seen to be small already. The difference obtained for the period of plume oscillations is less than 2%. Similarly an averaging interval of 300 s was determined to yield converged averages of all quantities. The bubble size was taken as 5.0 mm for the perforated plate sparger and 2.2 mm for the sintered disc sparger in accordance with the experiments of Buwa and Ranade (2002).

4 SIMULATION RESULTS

Since the different works summarized in section 2 use different combinations of parameters and provide different measured quantities, a suitable selection has to be made in order to keep the number of simulations within reasonable bounds while providing the best possible comparison with the experimental data. The test conditions chosen for the simulations are listed in Table 3. The available measurement data for each case will be discussed together with the comparison to the simulation results, first for the time-averaged phasic velocities and phase fractions, then for the plume oscillation period, which is a dynamic property of the flow.

test case	H/D	sparger	J_G	d_B
	-		cm/s	mm
N1	2.25	perforated plate	0.14	5.0
N2	2.25	perforated plate	0.16	5.0
N3	2.25	perforated plate	0.73	5.0
N4	4.5	perforated plate	0.16	5.0
N5	4.5	perforated plate	0.73	5.0
N6	2.25	perforated plate	0.30	5.0
N7	2.25	perforated plate	0.44	5.0
N8	2.25	perforated plate	0.59	5.0
N9	4.5	perforated plate	0.30	5.0
N10	4.5	perforated plate	0.44	5.0
N11	4.5	perforated plate	0.59	5.0
F1	2.25	sintered disc	0.16	2.2
F2	2.25	sintered disc	0.30	2.2
F3	2.25	sintered disc	0.44	2.2
F4	2.25	sintered disc	0.59	2.2
F5	2.25	sintered disc	0.73	2.2

Table 3: Summary of test conditions used for the simulations.

4.1 Average velocities and gas fraction

First, test case N1 is considered, for which lateral profiles of the liquid velocity are available at different heights (130, 250, and 370 mm) of the column from Pfleger et al. (1999) and at the highest level a gas fraction profile is available from Buwa and Ranade (2002). The gas volume flux for these experiments is $J_G = 0.14$ cm/s and the column aspect ratio is $H/D = 2.25$, exactly matching the values used in the simulations. Comparison of the measurements with the corresponding results of the present simulations is shown in Figure

2 and Figure 3, respectively. For the liquid velocity, good agreement is found at the lowest level, while at the higher levels, the simulations overestimate the peak value of the velocity in the center of the column as well as the recirculating velocity near the column walls. For the gas fraction, agreement between simulation and experiment is very good. A notable asymmetry between left and right halves of the experimental profiles for both liquid velocity and gas fraction points to the fact that averaging was performed over a too short time interval containing too few oscillation periods of the bubble plume. In the simulation results such an asymmetry is not seen.

A profile of gas velocity for conditions close to test case N5 (specifically $J_G = 0.7$ cm/s, $H/D = 5$, and $d_b = 5.5$ mm) is available from a previous study (Krauß and Rzehak, 2018). There, simulations were run using the same model as the present investigation and compared to experimental data from Darmana et al. (2007). Since these results nicely complement the present study, they are included in Figure 4. It can be seen that the peak of the calculated gas velocity matches the measurements very well, while the calculated values near the wall are too high in comparison.

For the test cases N2 to N5, further data on the gas fractions are available from Buwa and Ranade (2005). The experimental conditions comprise two values of the gas volume flux $J_G = 0.16$ and 0.73 cm/s, the lower of which is similar to that of test case N1, and two values of the column aspect ratio $H/D = 2.25$ and 4.5, again exactly matching the values used in the simulations. Measurements are taken at three levels as indicated in Figure 5, where they are compared to the corresponding simulation results. At the lowest level, the simulated profiles are too peaked. This effect is more pronounced for the higher value of the gas volume flux and for the lower value of the aspect ratio, where the measurement level is at a smaller fraction of the total fill height. At the higher levels, the simulations agree very well with the measurements for the lower value of the gas flux and both values of the aspect ratio. For the higher value of the gas flux the simulations tend to have too broad shoulders. At the lower value of the aspect ratio quantitative agreement with the experimental data is still good, but at the higher value of the aspect ratio significant deviations are seen.

To further elucidate this behavior, gas fraction profiles obtained from the simulations of all test cases N1 to N11 are shown in Figure 6 at the highest measurement level for both values of the aspect ratio. This includes further values of the gas volume flux intermediate to those of Figure 5 for which no measured gas fraction profiles are available. With increasing gas volume flux, the peak gas fraction obviously increases. At the same time however, the profile shape changes from a rather narrow peak to a broader shape with shoulders on each side. For the same value of the gas volume flux, the change is more pronounced at the higher value of the aspect ratio.

Finally, Figure 7 shows a comparison of the total gas fraction contained in the entire column for test cases N1-N3 and N6-N8, i.e. those with the lower value of the aspect ratio. For these conditions, experimental data are available from Diaz et al. (2006). The agreement between simulation and experiment for this quantity is very good.

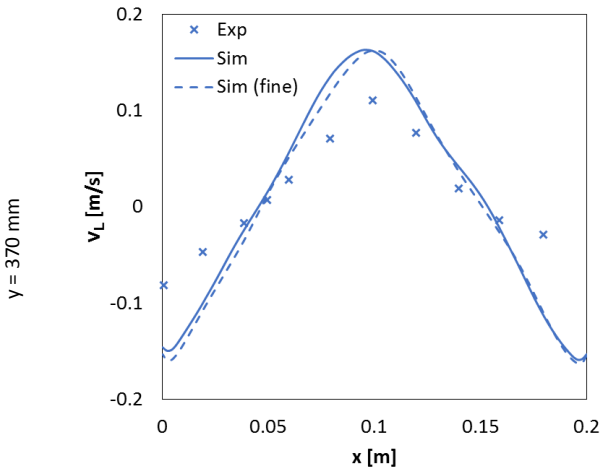

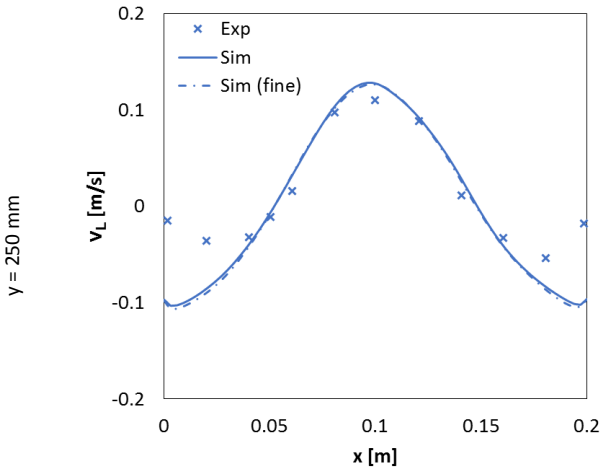

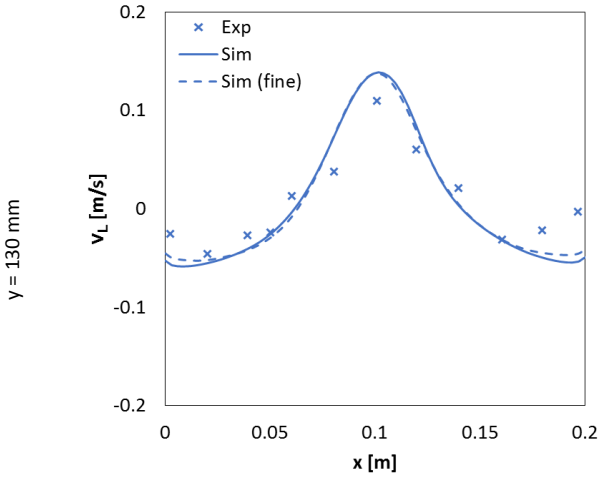

Figure 2: Vertical liquid velocity profiles for test N1. Symbols: experimental data from Pfleger et al. (1999); Lines: present simulation results (dashed lines for finer grid as described in section 3).

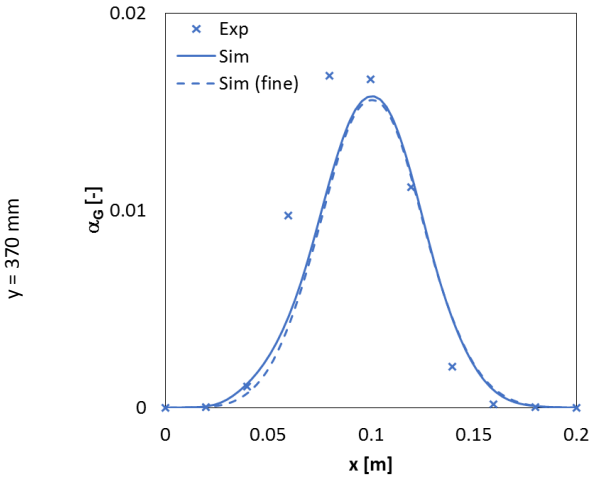

Figure 3: Gas fraction profile for test N1. Symbols: experimental data from Buwa and Ranade (2002); Lines: present simulation results (dashed line for finer grid as described in section 3).

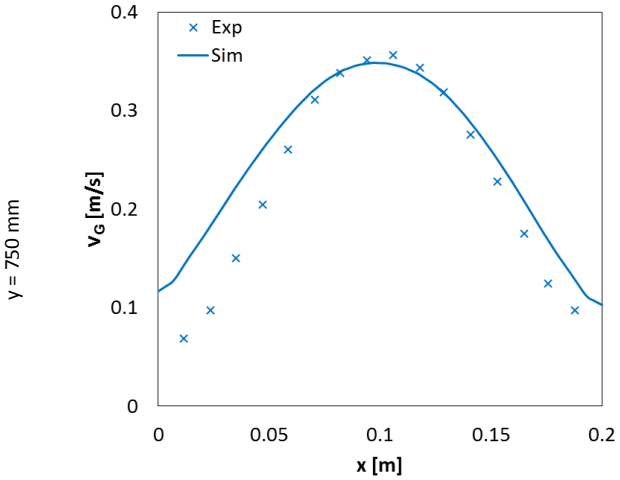

Figure 4: Vertical gas velocity profile for conditions close to test N5. Symbols: experimental data from Darmana et al. (2007); Lines: simulation results from Krauß and Rzehak (2018) using the same model as the present investigation.

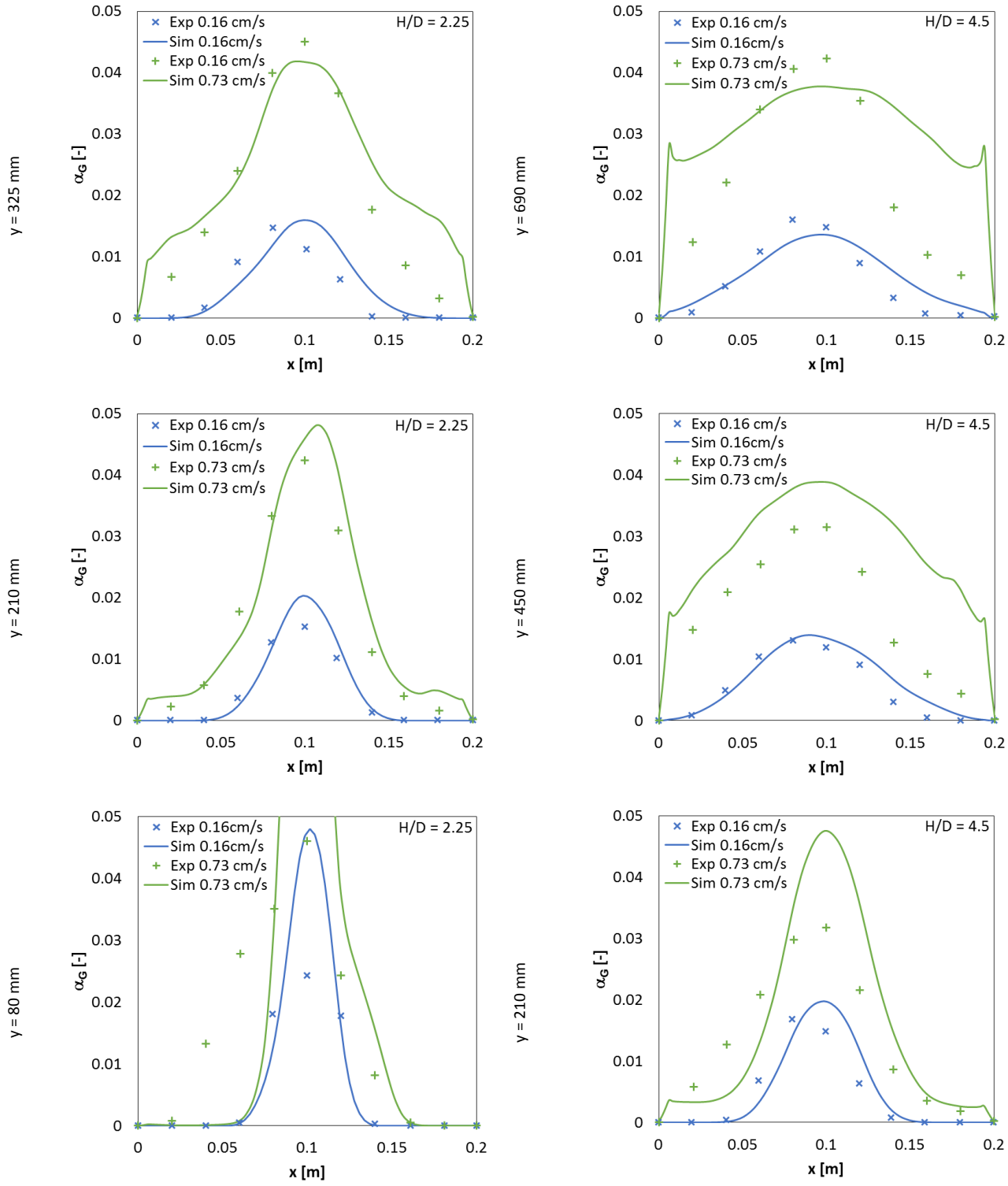

Figure 5: Gas fraction profiles for tests N2 to N5. Symbols: experimental data from Buwa and Ranade (2005); Lines: present simulation results.

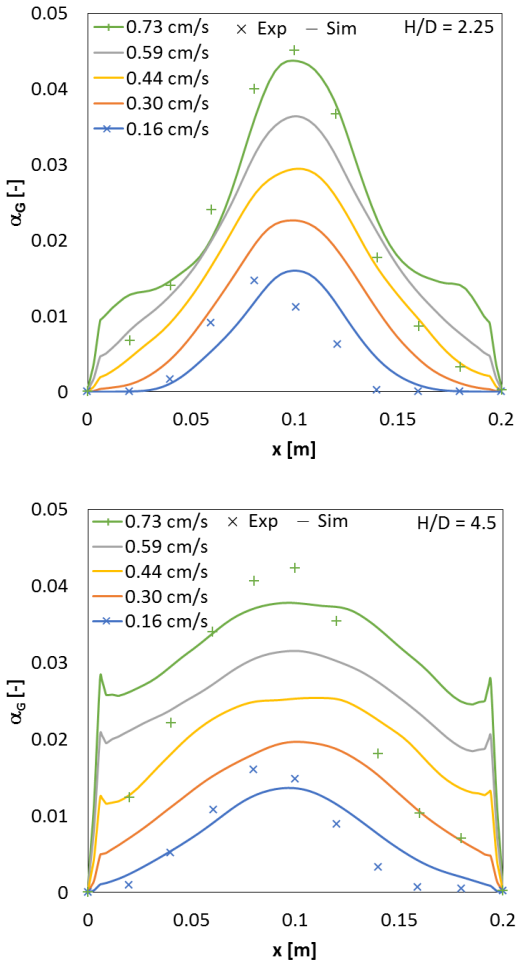

Figure 6: Simulated gas fraction profiles at the highest measurement level (lines) for all gas flow rates at H/D=2.25 (tests N1-N3 and N6-N8, top) and H/D=2.25 (tests N4-N5 and N9-N11, bottom). Experimental data (symbols) from Buwa and Ranade (2005) are added where available.

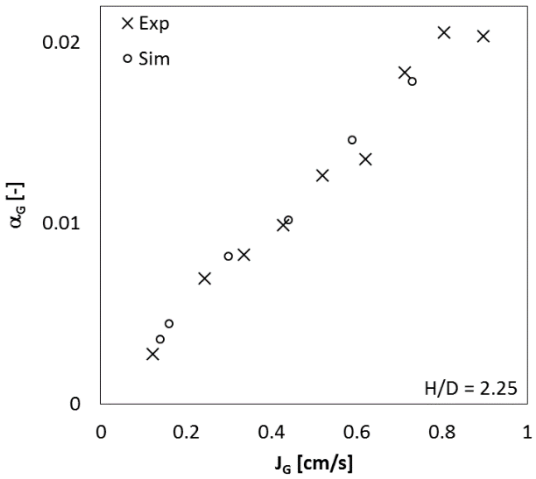

Figure 7: Total gas fraction inside the column for H/D=2.25 (tests N1-N3 and N6-N8) as function of gas volume flux. Crosses: experimental data from Diaz et al. (2006); Circles: present simulation results.

A possible origin of the deviations between simulations and experiments, which are found for the gas fractions at higher values of the gas volume flux and the higher value of the aspect ratio in Figure 5, is the occurrence of coalescence between the bubbles. This effect would increase with the gas volume flux due to the higher gas fraction. Also it would be more pronounced at higher aspect ratio since then the residence time of the bubbles is higher. Unfortunately, measurements of the distribution of the bubbles size at different heights of the column, which could unambiguously prove the occurrence of bubble coalescence, are not available. In the simulations this effect has been neglected to a first approximation, because models to describe it are not well-established as of yet. This is largely due to a general lack of the kind of data just mentioned, which are necessary to validate such models. Disagreement in the gas fraction near the inlet in Figure 5 can be attributed to a shortcoming in the inlet conditions.

An explanation of the deviations for the liquid velocities in Figure 2 is not obvious. This deviation is particularly surprising in view of the good agreement of the gas fractions for these experimental conditions and the fact that the deviations for the gas velocities in Figure 4 point in the other direction, i.e. a too high rather than too low value near the sidewalls of the column. The gas velocity being too high near the column walls in turn is at least consistent with the too broad gas fraction profile identified above as a possible consequence of the occurrence of bubble coalescence.

Comparison can also be made with the simulations of Buwa et al. (2002) based on a model quite similar to the present one. For case N1, these previous simulations also gave good agreement for the gas fractions, but the liquid velocity there was underpredicted, rather than overpredicted, by a similar amount. The good agreement of the gas fraction profile suggests that differences in the models applied for the non-drag forces are of minor importance. Differences in the bubble-induced turbulence modeling causing a different profile of turbulent viscosity thus remain as a likely cause for the deviations in the liquid velocity.

4.2 Plume oscillation period

For all considered test cases the period of plume oscillations (POP) was determined from the simulation results by averaging the time interval between zero crossings in a time series of the x-component of the liquid velocity at a point in the center of the column cross section at height $y = 250$ mm. A comparison with various experimental results is shown in Figure 8, in the left part for an aspect ratio $H/D = 2.25$ and in the right part for $H/D = 4.5$ in the present simulations. In the latter case, the experiments of Buwa and Ranade (2002) were taken at a slightly different value $H/D = 5.5$. Results from the previous study (Krauß and Rzehak, 2018) comparing simulation results based on the same model as in the present work to experimental data on the plume oscillations at $H/D = 5.0$ from Darmana et al. (2007) are also included.

Compared to the perforated plate sparger data from different sources at the lower value of the aspect ratio, there is quite good agreement for all values of J_G within the range of experimental uncertainty evidenced by the deviations between the different experimental data sets. At the lowest values of J_G, an error in the reported value of the gas volume flux could also be important since the dependence is rather steep. Compared to the sintered

disc sparger, which produces smaller bubbles, agreement is good for the lower values of J_G, but the simulation tends to underpredict the experimental data for $J_G \geq 0.4$. In this range also a different behavior between the two sparger types becomes visible in the experimental data: For the sintered disc sparger the POP tends to a constant value while it continually decreases for the perforated plate sparger. This behavior was explained by Buwa and Ranade (2002) by visual observations showing that the sintered disc sparger at higher flow rates produced very much larger bubbles than the perforated plate sparger. Moreover, it was suggested that this is due to coalescence near the sparger. This explanation again matches the present simulation results, where coalescence is neglected, but due to the lack of data on the bubble size distribution a direct verification is not feasible.

Comparing experimental data for the POP at different values of the aspect ratio it was noted by Buwa and Ranade (2004) that there is only a small influence at least in the range of parameters considered herein. This conclusion is confirmed by the present simulations, which give similar results for both values of the aspect ratio considered. Neglecting the small difference between the setups, good agreement between the present simulations and the experiment is also found for the higher value of the aspect ratio. Only the previous simulations of (Krauß and Rzehak, 2018) show a significant deviation from all other trends.

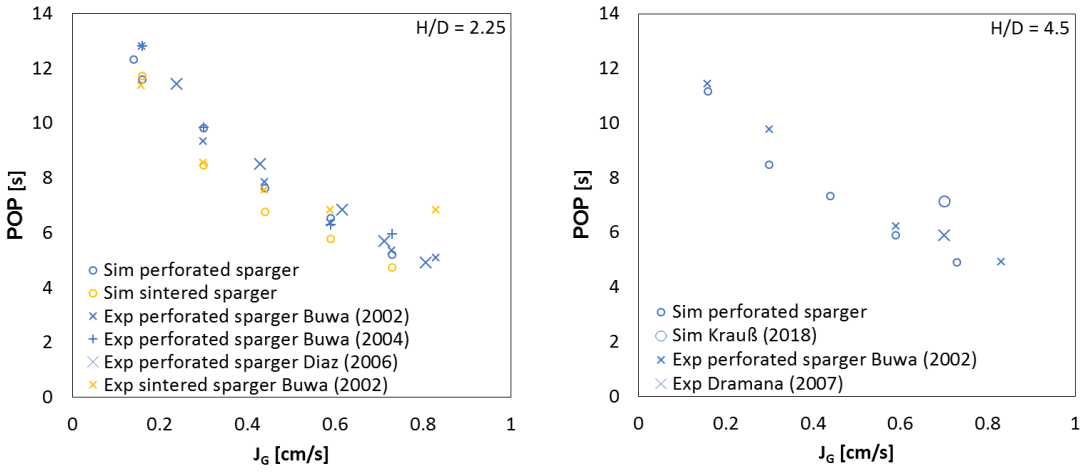

Figure 8: Period of plume oscillations for all tests. Left side: aspect ratio H/D=2.25; Right side aspect ratio H/D=4.5 in the present simulations, H/D=5.5 in the data of Buwa and Ranade (2002) and H/D=5.0 in the works of Krauß and Rzehak (2018) and Darmana et al (2007). Dark blue color: perforated plate sparger, light orange color: sintered disc sparger. Small crosses: experimental data from Buwa and Ranade (2002, 2004); Large crosses: experimental data from Diaz et al (2006) and Darmana et al (2007); Small circles: present simulation results; Large circle: simulation results from Krauß and Rzehak (2018).

5 CONCLUSIONS

A series of previous works to validate a single set of closure models for different bubbly flows has been extended to the case of an oscillating bubble plume as an example of a time-dependent flow. The overall agreement with the available experimental data was found quite good, in particular for the plume oscillation period. Part of the observed deviations could be due to the fact that a monodisperse approximation has been used for the simulations and bubble coalescence was neglected. Models needed to include such effects have not yet reached a stage where they can be relied on (Liao et al. 2015). In part this is due to the unavailability of data that resolve the bubble size distribution at different heights of a bubble column. Additional potential for model improvement is seen in the accurate description of bubble-induced turbulence. Despite the obvious possibilities for improvement, the proposed hydrodynamic closure models form a suitable basis to include further effects such as mass transfer (e.g. Rzehak 2016) and chemical reactions (e.g. Krauß and Rzehak 2017) for which there is a strong desire from the application side.

6 NOMENCLATURE

Symbol	Unit	Denomination
d_B	m	bubble diameter
D	m	column width
F	N m^{-3}	force per unit volume
g	m s^{-2}	acceleration of gravity
H	m	fill height of bubble column
J	m s^{-1}	superficial velocity = volumetric flux
k	m^2 s^{-2}	specific turbulent kinetic energy
p	N m^{-2}	pressure
POP	s	period of plume oscillations
t	s	time
T	m	column depth
$\mathbf{T}$	N m^{-2}	stress tensor
$\boldsymbol{u}$	m s^{-1}	mean velocity vector
v	m s^{-1}	mean vertical velocity
x	m	axial coordinate
y	m	vertical coordinate
z	m	spanwise coordinate
α	-	phase fraction
ϵ	m^2 s^{-3}	turbulent dissipation rate
μ	kg m^{-1} s^{-1}	dynamic viscosity
ρ	kg m^{-3}	density

σ	N m^{-1}	surface tension
ω	s^{-1}	turbulent frequency

Index	Denomination
$turb$	turbulent
G	gas phase
$inter$	at interface
L	liquid phase

7 REFERENCES

Becker, S., Bie, H. D., and Sweeney, J., 1999. Dynamic flow behaviour in bubble columns. *Chemical Engineering Science* 54, 4929–4935.

Burns, A. D., Frank, T., Hamill, I., Shi, J.-M., 2004. The Favre averaged drag model for turbulence dispersion in Eulerian multi-phase flows. *Proc. 5th Int. Conf. on Multiphase Flow*, ICMF2004, Yokohama, Japan.

Buwa, V. V., and Ranade, V. V., 2002. Dynamics of gas-liquid flow in a rectangular bubble column: Experiments and single/multi-group CFD simulations. *Chemical Engineering Science* 57, 4715–4736.

Buwa, V. V., and Ranade, V. V., 2004. Characterization of dynamics of gas–liquid flows in rectangular bubble columns. *AIChE Journal* 50, 2394–2407.

Buwa, V. V., and Ranade, V. V., 2005. Characterization of gas-liquid flows in rectangular bubble columns using conductivity probes. *Chemical Engineering Communications* 192, 1129–1150.

Buwa, V. V., Deo, D. S., and Ranade, V. V., 2006. Eulerian-Lagrangian simulations of unsteady gas-liquid flows in bubble columns. *International Journal of Multiphase Flow* 32, 864–885.

Cachaza, E. M., Diaz, M. E., Montes, F. J., and Galan, M. A., 2011. Unified study of flow regimes and gas holdup in the presence of positive and negative surfactants in a non-uniformly aerated bubble column. *Chemical Engineering Science* 66, 4047–4058.

Darmana, D., Henket, R., Deen, N., Kuipers, J., 2007 Detailed modelling of hydrodynamics, mass transfer and chemical reactions in a bubble column using a discrete bubble model. *Chemical Engineering Science* 62, 2556–2575.

Delnoij, E., Kuipers, J. H., and Swaaij, van W. W., 1997. Dynamic simulation of gas-liquid two-phase flow: effect of column aspect ratio on the flow structure. *Chemical Engineering Science* 52, 3759–3772.

Diaz, M. E., Montes, F. J., and Galan, M. A., 2006. Influence of Aspect Ratio and Superficial Gas Velocity on the Evolution of Unsteady Flow Structures and Flow Transitions in a Rectangular Two-Dimensional Bubble Column. *Industrial & Engineering Chemistry Research* 45, 7301–7312.

Diaz, M. E., Iranzo, A., Cuadra, D., Barbero, R., Montes, F. J., and Galan, M. A., 2008. Numerical simulation of the gas–liquid flow in a laboratory scale bubble column: Influence of bubble size distribution and non-drag forces. *Chemical Engineering Journal* 139, 363–379.

Drew, D. A., Passman, S. L., 1998. Theory of Multicomponent Fluids, *Springer*.

Gupta, A. and Roy, S., 2013. Euler–Euler simulation of bubbly flow in a rectangular bubble column: Experimental validation with Radioactive Particle Tracking. *Chemical Engineering Journal* 225, 818–836.

Hosokawa, S., Tomiyama, A., Misaki, S. and Hamada, T., 2002. Lateral migration of single bubbles due to the presence of wall. *Proc. ASME Joint U.S.-European Fluids Engineering Division Conference,* FEDSM2002*,* Montreal, Canada.

Ishii, M. and Hibiki, T., 2011. Thermo-fluid dynamics of two-phase flow. *Springer*, 2nd ed.

Ishii, M. and Zuber, N., 1979. Drag coefficient and relative velocity in bubbly, droplet or particulate flows. *AIChE Journal* 25, 843–855.

Julia, J. E., Hernandez, L., Chiva, S., and Vela, A., 2007. Hydrodynamic characterization of a needle sparger rectangular bubble column: Homogeneous flow, static bubble plume and oscillating bubble plume. *Chemical Engineering Science* 62, 6361–6377.

Krauß, M. and Rzehak, R., 2017. Reactive absorption of CO2 in NaOH: Detailed study of enhancement-factor models. *Chemical Engineering Science* 166, 193–209.

Krauß, M. and Rzehak, R., 2018. Reactive absorption of CO2 in NaOH: An Euler-Euler simulation study. *Chemical Engineering Science* 181, 199–214.

Laupsien, D., Cockx, A., and Line, A., 2017. Bubble plume oscillations in viscous fluids. *Chemical Engineering & Technology* 40, 1484–1493.

Liao, Y., Rzehak, R., Lucas, D. and Krepper, E., 2015. Baseline Closure Model for Dispersed Bubbly Flow: Bubble-Coalescence and Breakup. *Chemical Engineering Science* 122, 336–349.

Liao, J., Ziegenhein, T., and Rzehak, R., 2016. Bubbly flow in an airlift column: A CFD study. *Journal of Chemical Technology & Biotechnology* 91, 2904–2915.

Lin, T.-J., Reese, J., Hong, T., and Fan, L.-S., 1996. Quantitative analysis and computation of two-dimensional bubble columns. *AIChE Journal* 42, 301–318.

Liu, L., Yan, H., Ziegenhein, T., Hessenkemper, H., Li, Q., Lucas, D., 2019. A systematic experimental study and dimensionless analysis of bubble plume oscillations in rectangular bubble columns. *Chemical Engineering Science,* under consideration*.*

Parekh, J. and Rzehak, R., 2018. Euler-Euler multiphase CFD-simulation with full Reynolds stress model and anisotropic bubble-induced turbulence. *International Journal of Multiphase Flow* 99, 231–245.

Pfleger, D., Gomes, S., Gilbert, N., and Wagner, H.-G., 1999. Hydrodynamic simulations of laboratory scale bubble columns fundamental studies of the Eulerian–Eulerian modelling approach. *Chemical Engineering Science* 54, 5091–5099.

Rensen, J. M., and Roig, V., 2001. Experimental study of the unsteady structure of a confined bubble plume. *International Journal of Multiphase Flow* 27, 1431–1449.

Rzehak, R. 2016. Modeling of mass-transfer in bubbly flows encompassing different mechanisms. *Chemical Engineering Science* 151, 139–143.

Rzehak, R., Krauß, M., Kovats, P., and Zähringer, K., 2017a. Fluid dynamics in a bubble column: New experiments and simulations. *International Journal of Multiphase Flow* 89, 299–312.

Rzehak, R. and Krepper, E., 2013. Bubble-induced turbulence: Comparison of CFD models. *Nuclear Engineering and Design* 258, 57–65.

Rzehak, R. and Krepper, E., 2013a. CFD modeling of bubble-induced turbulence. *International Journal of Multiphase Flow* 55, 138–155.

Rzehak, R. and Krepper, E., 2015. Bubbly flows with fixed polydispersity: Validation of a baseline closure model. *Nuclear Engineering and Design* 287, 108–118.

Rzehak, R., Krepper, E., Liao, Y., Ziegenhein, T., Kriebitzsch, S. and Lucas, D., 2015. Baseline model for the simulation of bubbly flows. *Chemical Engineering and Technology* 38, 1972–1978.

Rzehak, R., Krepper, E., 2016. Euler-Euler simulation of mass-transfer in bubbly flows. *Chemical Engineering Science* 155, 459–568.

Rzehak, R. and Kriebitzsch, S., 2015. Multiphase CFD-simulation of bubbly pipe flow: A code comparison. *International Journal of Multiphase Flow* 68, 135–152.

Rzehak, R., Ziegenhein, T., Kriebitzsch, S., Krepper, E., and Lucas, D., 2017. Unified modeling of bubbly flows in pipes, bubble columns, and airlift columns. *Chemical Engineering Science* 157, 147–158.

Shi, P. and Rzehak, R., 2017. Bubbly flow in stirred tanks: Euler-Euler / RANS modeling. *Chemical Engineering Science* 190, 419–435.

Tomiyama, A., Tamai, H., Zun, I., and Hosokawa, S., 2002. Transverse migration of single bubbles in simple shear flows. *Chemical Engineering Science* 57, 1849–1858.

Upadhyay, R. K., Pant, H. J., and Roy, S., 2013. Liquid flow patterns in rectangular air-water bubble column investigated with Radioactive Particle Tracking. *Chemical Engineering Science* 96, 152–164.

Yeoh, G. H. and Tu, J. Y., 2010. Computational Techniques for Multiphase Flows — Basics and Applications, *Butterworth-Heinemann*.

Ziegenhein, T., Rzehak, R., Krepper, E. and Lucas, D., 2013. Numerical simulation of polydispersed flow in bubble-columns with the inhomogeneous multi-size-group model. *Chemie Ingenieur Technik* 85, 1080–1091.

Ziegenhein, T., Rzehak, R., Ma, T., and Lucas, D., 2017. A unified approach for modeling uniform and non-uniform bubbly flows. *Canadian Journal of Chemical Engineering* 95, 170–179.